Journal of Alloys and Compounds 628 (2015) 208–212

Contents lists available at ScienceDirect

Journal of Alloys and Compounds

journal homepage: www.elsevier.com/locate/jalcom

Letter

Novel method to fabricate Ti–Al intermetallic compound coatings on Ti–6Al–4V alloy by combined ultrasonic impact treatment and electrospark deposition

Yang Liu, Dongpo Wang, Caiyan Deng *, Lixing Huo, Lijun Wang, Rui Fang

Tianjin Key Laboratory of Advanced Joining Technology, School of Materials Science and Engineering, Tianjin University, Tianjin 300072, PR China

ARTICLE INFO

Article history:
Received 11 July 2014
Received in revised form 18 November 2014
Accepted 13 December 2014
Available online 31 December 2014

Keywords:
Coating
Ultrasonic impact treatment
Intermetallics
X-ray photoelectron spectroscopy
Residual stress

ABSTRACT

A Ti–Al intermetallic compound coating was fabricated on Ti–6Al–4V alloy by combined ultrasonic impact treatment and electrospark deposition. The principle of the combined process is described in detail based on studies of the chemical states, microstructure, phase compositions, microhardness, and surface residual stress of the coating. Many new Ti–Al intermetallic compounds distinct from the deposition materials are found to make up the coating, along with a small amount of Al_2O_3. The high energy of the electrospark facilitates the chemical reactions among elements. Further, the impact process produces a plastic deformation layer. The microhardness of the Ti–6Al–4V under the coating also increased because of the plastic deformation layer. Finally, the surface residual stress of samples treated by the combined process is compressive stress.

1. Introduction

Titanium and its alloys are widely used in aviation and space technology because of their excellent mechanical properties (high strength and fatigue resistance) and chemical stability (corrosion resistance). However, titanium alloys have poor tribological properties, which reduces their scope of possible usage [1]. To enhance the wear resistance of the material, many surface modification methods have been developed, such as powder sintering [2], electrospark deposition [3], physical vapor deposition [4], plasma immersion ion implantation [5], microarc discharge oxidation [6], and laser diffusion nitriding [7].

Ultrasonic impact treatment (UIT) [8] was originally developed as a method to relax residual welding stress, reduce the stress concentration coefficient of the weld toe, and form compressive residual stress to improve the fatigue performance of welded structures [9–15]. In recent years, however, UIT and its variants have also been used for surface modification of materials [16–18]. However, because UIT is a surface mechanical treatment and can hardly alter the elemental composition of alloy, the application range of UIT surface modification is significantly limited. Compared to UIT, electrospark deposition can easily transfer electrode materials or other elements to the target. However, a molten pool is created during conventional electrospark deposition, and the tensile residual stress in the coating due to the solidification of the molten pool can have large potential negative effects on the alloy's wear, fatigue, and stress corrosion performance [19].

The available experimental data show that the aluminide phases of the Ti–Al system can be used as protective layers for industrial titanium alloys [20]. In particular, the intermetallic compounds Ti_3Al, TiAl, and $TiAl_3$ have a number of unique properties and can improve the surface hardness and wear resistance of titanium alloys [21].

This work explores the feasibility of the fabrication of Ti–Al intermetallic compound coatings on Ti–6Al–4V alloy by combined UIT and electrospark deposition (ultrasonic impact electrospark treatment, UIET). Moreover, the principle of UIET is described.

2. Experimental

A custom-developed machine for UIET was used to fabricate the coatings. A typical photograph showing the UIET process is provided in Fig. 1a, and the schematic diagram of the experimental setup for evaluating the UIET principle is given in Fig. 1b. In this setup, the ultrasonic transducer converts electrical energy from the ultrasonic generator into ultrasonic vibration with a frequency of 20 kHz. Under a static pressure, the shock ball vibrates rapidly between the ultrasonic transducer and the target surface. To combine the electrospark process with UIT, the shock ball and target were connected to the anode and cathode, respectively, of a DC power source. The DC power source, shock ball, target, and wires composed the electrospark circuit. The impact signals and current signals of the electrospark circuit were collected by a double-channel oscilloscope.

The principle of UIET is shown in Fig. 2. The top half of Fig. 2a shows the voltage signals collected from the piezoelectric force-measuring element, which represent the impacts on the target. The bottom half of Fig. 2a shows the current signals of

* Corresponding author. Fax: +86 22 27405889.
E-mail address: dengcaiyan@tju.edu.cn (C. Deng).

http://dx.doi.org/10.1016/j.jallcom.2014.12.144
0925-8388/

the electrospark circuit. When the shock ball impacts the target, the piezoelectric force-measuring element outputs a pulse signal. At the same moment, the current value of electrospark circuit is about the short-circuit current (see A in Fig. 2a and the impact process in Fig. 2b). The midpoint between two neighboring pulses corresponds to the moment when the shock ball bounces. At this point, the current value of the electrospark circuit decreases to about 6 A, which indicates that an electrospark is produced between the shock ball and the target (see B in Fig. 2a and the electrospark process in Fig. 2b). This decrease in current occurs because the electrospark increases the total resistance of the circuit. Every impact corresponds to one short circuit, and every bounce corresponds to one electrospark. The impact and electrospark processes continue in cycles, which constitute the UIET process. From Fig. 2a, it can be seen that the frequency of UIET is 6 kHz, i.e., the time of every UIET cycle is about 167 μs.

As in UIT, during the impact process, various changes occur in the target surface, such as plastic deformation and the introduction of compressive residual stress [10]. The ultrasonic transducer used is a piezoelectric ceramic transducer, and the excitation signal is a sine wave signal, i.e., a continuous excitation signal. The calculation results obtained using the calculation method reported by Statnikov et al. for the estimation of the ultrasonic transducer energy utilization [8] are as follows: the ultrasonic transducer vibration frequency is 20 kHz, the impact frequency is 6 kHz, and the impact efficiency of UIET is 30%.

During the electrospark process, the arc heat melts the electrospark poles, i.e., parts of the shock ball and the target surface. A microscale molten pool is formed on the surface of the target. Due to the effect of gravity, the molten parts of the shock ball fall into the microscale molten pool. Further, the cooling liquid and air in the electrospark area are ionized. Thus, there are many elements from the substrate, electrode, cooling liquid, and air in the microscale molten pool, which together provide the appropriate mix and reactions of chemicals (see the partial enlargement of the area around the molten pool in Fig. 2b). During the subsequent impact process, the electrospark is extinguished. The surrounding cooling liquid causes rapid (microsecond) solidification of the microscale molten pool, i.e., the formation of the coatings.

A Ti–6Al–4V substrate with the thickness of 3 mm was cut into a rectangle with dimensions of 300 mm × 300 mm and ground using SiC abrasive paper to a 600 grit finish for UIET. The shock ball was made of TiAl alloy and had a diameter of 15 mm. Its chemical composition (in at%) was 45.29% Al, 46.85% Ti, and 7.86% V. The amplitude of the ultrasonic transducer was 25 μm. The static pressure was 100 N. The short-circuit current of the electrospark circuit was 22 A. The cooling liquid was the cutting fluid for electrical discharge machining. X-ray photoelectron spectroscopy (XPS) measurements were performed with a Kratos Axis Ultra DLD. The cross-sectional microstructure and elemental composition of samples were investigated by SEM and EDX, respectively. The phase compositions and surface residual stress of samples were studied by XRD. The microhardness was measured by a digital microhardness tester (MHV-2000) under an applied load of 0.49 N for a load time of 15 s. The depth profiles of the subsurface microhardness were determined by successive electrolytic material removal.

3. Results and discussion

XPS surface analysis of the Ti–6Al–4V alloy after UIET revealed the presence of the main constituents Ti, Al, O, C, and N. Fig. 3 shows fitted Ti 2*p*, Al 2*p*, O 1*s*, C 1*s*, and N 1*s* high-resolution XP

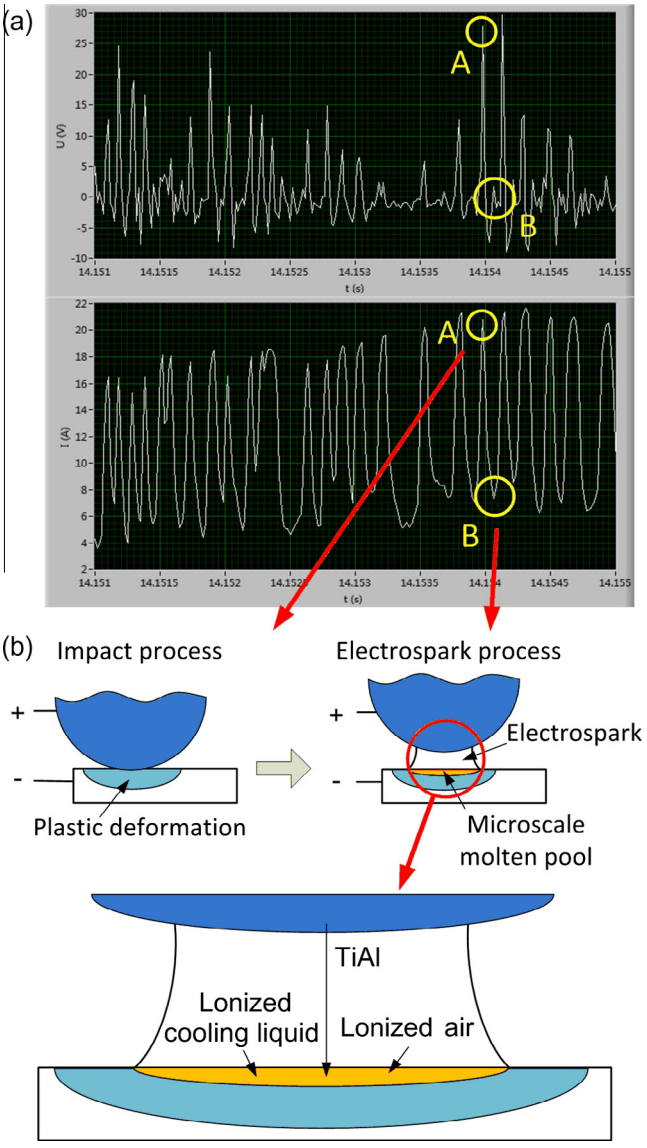

Fig. 2. (a) Oscilloscope readout showing impacts and current of the electrospark circuit and (b) principle of UIET.

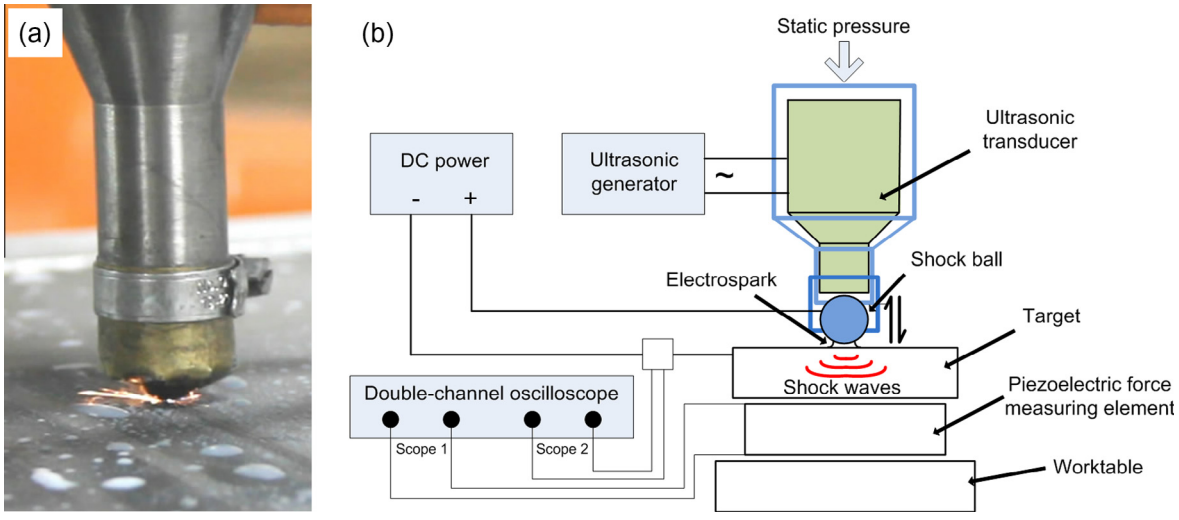

Fig. 1. (a) Typical photograph of the UIET process and (b) schematic diagram of experimental setup for evaluating the UIET principle.

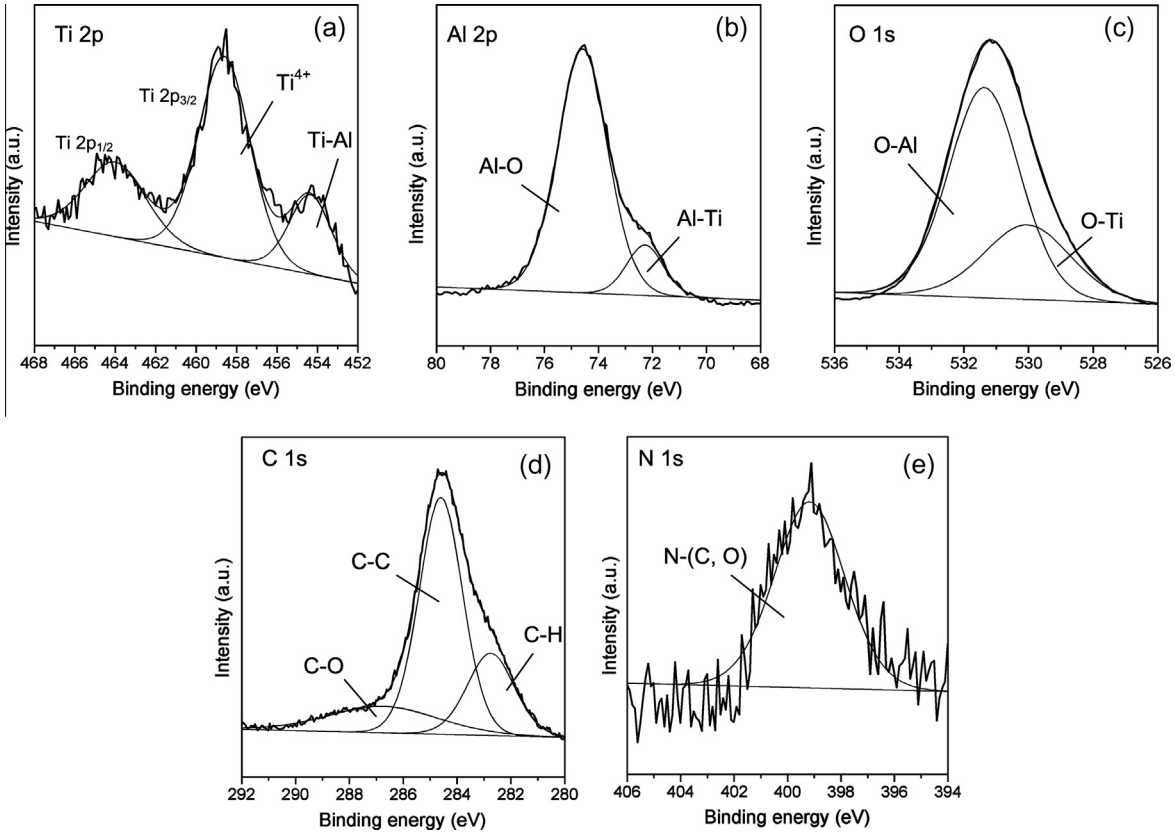

Fig. 3. Curve-fitted (a) Ti 2*p*, (b) Al 2*p*, (c) O 1*s*, (d) C 1*s*, and (e) N 1*s* X-ray photoelectron core-level spectra of Ti–6Al–4V alloy after UIET.

spectra of the alloy after UIET. The complex Ti $2p_{3/2}$ peak envelope of the treated sample could be adequately synthesized by using doublets of two components (Fig. 3a). The Ti $2p_{3/2}$ binding energy (BE) = 454.10 eV of the minor component in the Ti $2p_{3/2}$ spectrum (about 17.4% of the total peak area) is in accordance with data reported for Ti–Al bonds [22]. In addition, the Ti $2p_{3/2}$ peak at 458.65 eV with a fraction of about 82.6% can be ascribed to Ti^{4+} in TiO_2. Similarly to the Ti 2*p* spectrum, the Al 2*p* spectrum contains an intense peak dominated by the component at BE = 74.59 eV, which is associated with the Al–O bond [23]. According to data collected in Ref. [22], the minor component at 72.22 eV in the Al 2*p* envelope, corresponding to Al–Ti bond, is consistent with the presence of the Ti–Al component in the Ti 2*p* spectra (cf. Fig. 3a and b) and provides direct evidence for the formation of an Ti–Al intermetallic compound on the alloy surface. Deconvolution of the O 1*s* peak allowed identification of two different chemical states of oxygen on the alloy surface (Fig. 3c). The largest component (about 70% of the peak area) at BE = 531.36 eV is obviously related to the O^{2-} ions in the aluminum oxide [24]. The minor component at BE = 530.03 eV falls in the range of BEs reported for TiO_2 [25,26]. The C 1*s* line is broad and displays a distinct shoulder at BE = 283 eV (Fig. 3d). To fit this band, at least three components were required. These components at 284.60, 282.75, and 286.74 eV correspond to C–C, C–H and C–O species, respectively, and indicate strong contamination of the surface by hydrocarbons. A small N 1*s* peak detected on the surface is composed of one component located at 399.17 eV, which can result from the presence of chemisorbed N–C and N–O bonds. The results above establish that Ti–Al intermetallic compounds indeed form in the alloy during UIET.

After UIET, the sample consisted of an outer coating and an inner plastic deformation layer (see Fig. 4a). The coating has a thickness of 10–15 μm, is very compact without obvious cracks, and is bonded to the plastic deformation layer tightly. Local EDX microanalysis results of coating are shown in Table 1. Spectrum 1 is from the coating, which mainly consists of very large amounts of aluminum and vanadium, along with titanium and oxygen. However, the proportion of aluminum in the coating is less than that in the shock ball. This indicates that the melted shock ball material is mixed with substrate metal in the microscale molten pool created by the electrospark. Spectrum 2 is from the plastic deformation layer. The composition indicated by spectrum 2 is no different from the composition of Ti–6Al–4V alloy. The distributions of the main elements in the coating and plastic deformation layer, titanium and aluminum, were measured by elemental line scanning, as shown in Fig. 4b. A transition layer with a thickness of several microns is apparent, which confirms the metallurgical bonding between the coating and plastic deformation layer. The presence of elements from the substrate in the coating coming also proves the good metallurgical bonding between the coating and plastic deformation layer. The EDX results demonstrate that titanium and aluminum are transferred from the shock ball to the microscale molten pool on the target surface and are mixed with the substrate during UIET.

Fig. 5 shows the X-ray diffraction patterns of the substrate, shock ball, and sample after UIET. From these results, it can be seen that the shock ball (TiAl alloy) is mainly composed of TiAl and Ti_3Al. After UIET, new intermetallic compound peaks (mainly $TiAl_3$ and Ti_3Al) distinct from those from the substrate and shock ball were observed on the modified surface. This illustrates that drastic chemical reactions occur among elements in the microscale molten pool during the electrospark process. Furthermore, a small quantity of Al_2O_3 is formed on the modified surface, which is consistent with the Al 2*p* and O 1*s* peaks in the XPS results (see Fig. 3b and c). The coating is heterogeneous in the depth direction because of the rapid solidification of the coating. Therefore, the proportions of the

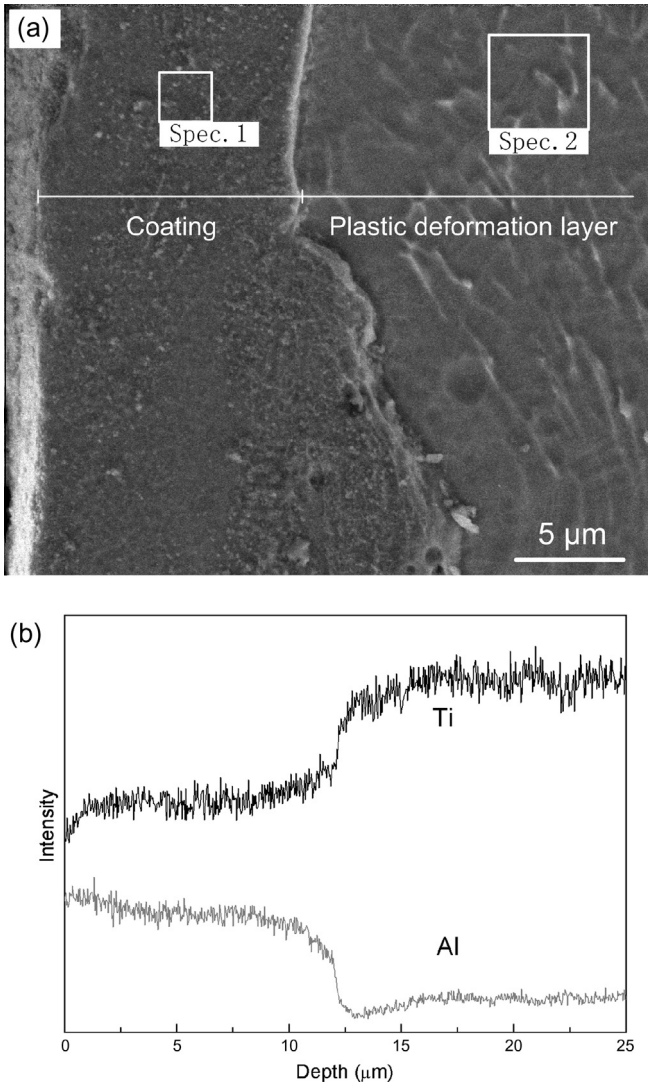

Fig. 4. (a) Cross-sectional microstructure and (b) titanium/aluminum distribution along the depth direction of the Ti–6Al–4V alloy after UIET.

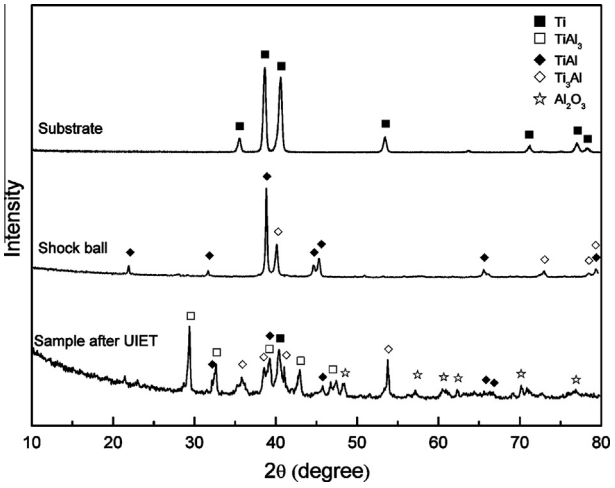

Fig. 5. XRD spectra of the substrate, shock ball, and sample after UIET.

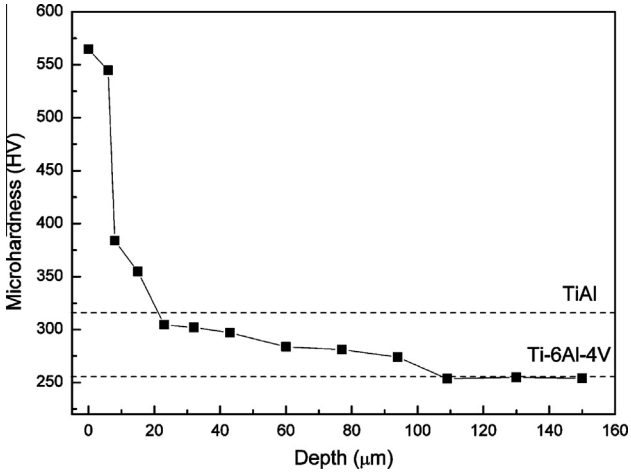

Fig. 6. Microhardness profiles of the sample after UIET.

Table 1
EDX-derived atomic concentrations of elements in the cross section of Ti–6Al–4V alloy after UIET (at%).

Spectrum	Ti	Al	V	O
1	49.99	36.79	6.48	6.74
2	86.57	11.74	1.69	0.00

components are different in the XPS and XRD results, while the components of the coating are the same (cf. Figs. 3 and 5).

The microhardness profile along the depth of the sample after UIET is given in Fig. 6. The maximum microhardness is about 540 HV on the top of the modified surface. As the depth increases to 8 μm, the microhardness falls sharply to about 380 HV. When the depth increases from 20 to 110 μm, the microhardness starts below the microhardness of TiAl alloy (shock ball material) and drops slowly to the microhardness of substrate (Ti–6Al–4V). When the depth is greater than 110 μm, the microhardness is stable. As shown in Fig. 4a, the thickness of coating is 10–15 μm. The indentation depths of first two test points are in the coating, so these two values are similar. After the depth is greater than 8 μm, the tip of the indenter penetrates the coating, so the microhardness is influenced by both the coating and plastic deformation layer. When the depth is greater than 20 μm, all the coating has been removed. Therefore, the slow fall in the microhardness at these depths is only due to the plastic deformation layer. The amount of plastic deformation in this layer gradually decreases from large to small along the depth [16,27]. When the depth is greater than 110 μm, the microhardness is similar to that of the substrate, because there is no plastic deformation. The microhardness of the coating is 70% higher than the microhardness of the TiAl alloy (shock ball). This illustrates that the increase in coating microhardness is due not only to the deposition of TiAl alloy, but also to the multiform complicated intermetallic components (see Fig. 5) in the microscale molten pool and the possible fine grains or high dislocation density of the coating [28,29]. Such fine grains could be ascribed to the vigorous reaction during the electrospark process, and the mechanical impacts during the impact process may lead to such a high dislocation density [16] (see Fig. 2b). According to reports on previous studies, the grain size decreases greatly with increasing cooling rate because of the large undercooling and the reduced solidification time prior to solidification [30,31]. With increasing cooling rate, the grain size of the alloy decreases greatly, and consequently, the hardness increases [31]. Based on the discussion above, the microhardness profile can be divided into the

sections corresponding to the coating, plastic deformation layer, and substrate.

The residual stress in coatings has been studied extensively [19]. Ahmaniemi et al. found that residual stress states were correlated with other coating properties such as the microhardness, porosity, microstructure, and dry abrasion wear resistance [32]. Compared to the conventional coating process, UIET has the significant advantage of producing a large compressive residual stress in the coatings. After UIET, the surface residual stress of the sample is −585.89 MPa, which may be beneficial for improving the wear [33], fatigue [11], and stress corrosion [34] resistance of the coatings.

4. Conclusions

A Ti–Al intermetallic compound coating was fabricated on Ti–6Al–4V alloy using UIET, and the principle of UIET was described in detail. A dense coating layer with a thickness of about 12 μm was obtained, and a plastic deformation layer was observed under the coating. Metallurgical bonding between the coating and plastic deformation layer was established. In particular, new Ti–Al intermetallic compound phases were obtained in the coating. The microhardness of coating was higher than that of the material of the shock ball (TiAl alloy), and the microhardness under the coating was also increased. Additionally, the surface residual stress of sample after UIET was compressive stress. Thus, UIET may be beneficial for improving the wear, fatigue, and stress corrosion resistance of various coatings.

Acknowledgement

The authors are grateful for support by the National Natural Science Foundation of China (Grant Nos. 51275343 and 51375331).

Appendix A. Supplementary material

Supplementary data associated with this article can be found, in the online version, at http://dx.doi.org/10.1016/j.jallcom.2014.12.144.

References

[1] P. Budzynski, A.A. Youssef, J. Sielanko, Wear 261 (2006) 1271–1276.
[2] R.-H. Hu, J.-K. Lim, Mater. Des. 31 (2010) 2670–2675.
[3] Y. Xie, M. Wang, J. Alloys Comp. 484 (2009) 21–24.
[4] Z. Xu, L. He, R. Mu, X. Zhong, Y. Zhang, J. Zhang, X. Cao, J. Alloys Comp. 473 (2009) 509–515.
[5] Y.L. Pei, Y. Luan, J. Alloys Comp. 581 (2013) 873–876.
[6] A. Polat, M. Makaraci, M. Usta, J. Alloys Comp. 504 (2010) 519–526.
[7] H.C. Man, M. Bai, F.T. Cheng, Appl. Surf. Sci. 258 (2011) 436–441.
[8] E.S. Statnikov, O.V. Korolkov, V.N. Vityazev, Ultrasonics 44 (2006) e533–e538.
[9] S. Roy, J.W. Fisher, B.T. Yen, Int. J. Fatigue 25 (2003) 1239–1247.
[10] B.N. Mordyuk, G.I. Prokopenko, J. Sound Vib. 308 (2007) 855–866.
[11] T. Wang, D. Wang, L. Huo, Y. Zhang, Int. J. Fatigue 31 (2009) 644–650.
[12] X. Zhao, D. Wang, L. Huo, Mater. Des. 32 (2011) 88–96.
[13] A. Berg-Pollack, F.J. Voellmecke, C.M. Sonsino, Int. J. Fatigue 33 (2011) 513–518.
[14] R.T. Yekta, K. Ghahremani, S. Walbridge, Int. J. Fatigue 55 (2013) 245–256.
[15] Y. Liu, D. Wang, C. Deng, L. Xia, L. Huo, L. Wang, B. Gong, Int. J. Fatigue 66 (2014) 155–160.
[16] W. Ting, W. Dongpo, L. Gang, G. Baoming, S. Ningxia, Appl. Surf. Sci. 255 (2008) 1824–1829.
[17] B.N. Mordyuk, M.O. Iefimov, G.I. Prokopenko, T.V. Golub, M.I. Danylenko, Surf. Coat. Technol. 204 (2010) 1590–1598.
[18] M.A. Vasylyev, S.P. Chenakin, L.F. Yatsenko, Acta Mater. 60 (2012) 6223–6233.
[19] A.C.G. Montay, A. Nussair, J. Lu, J. Mater. Sci. Technol. 20 (2004) 81–84.
[20] H. Garbacz, P. Wieciński, M. Ossowski, M.G. Ortore, T. Wierzchoń, K.J. Kurzydłowski, Surf. Coat. Technol. 202 (2008) 2453–2457.
[21] M.S. Chu, S.K. Wu, Surf. Coat. Technol. 179 (2004) 257–264.
[22] D.E. Mencer Jr., T.R. Hess, T. Mebrahtu, D.L. Cocke, D.G. Naugle, J. Vac. Sci. Technol. A 9 (1991) 1610–1615.
[23] K. Arata, M. Hino, Appl. Catal. 59 (1990) 197–204.
[24] E. Payen, L. Gengembre, F. Mauge, J.C. Duchet, J.C. Lavalley, Catal. Today 10 (1991) 521–539.
[25] I. Bertoti, M. Mohai, J. Sullivan, S. Saied, Appl. Surf. Sci. 84 (1995) 357–371.
[26] P.O. Larsson, A. Andersson, L.R. Wallenberg, B. Svensson, J. Catal. 163 (1996) 279–293.
[27] M. Yasuoka, P. Wang, K. Zhang, Z. Qiu, K. Kusaka, Y.-S. Pyoun, R.-I. Murakami, Surf. Coat. Technol. 218 (2013) 93–98.
[28] G. Liu, J. Lu, K. Lu, Mater. Sci. Eng. A 286 (2000) 91–95.
[29] A. Amanov, O.V. Penkov, Y.-S. Pyun, D.-E. Kim, Tribol. Int. 54 (2012) 106–113.
[30] David W. Heard, Julien Boselli, Roberto Rioja, Emmanuelle A. Marquis, Raynald Gauvin, Mathieu Brochu, Acta Mater. 61 (2013) 1571–1580.
[31] W.A.N.G. Hong-wei, Z.H.U. Dong-dong, Z.O.U. Chun-ming, W.E.I. Zun-jie, Trans. Nonferr. Met. Soc. China 21 (2011) s328–s332.
[32] S. Ahmaniemi, M. Vippola, P. Vuoristo, T. Mäntylä, M. Buchmann, R. Gadow, Wear 252 (2002) 614–623.
[33] C.E.J. Dancer, N.A. Yahya, T. Berndt, R.I. Todd, G. de Portu, Tribol. Int. 74 (2014) 87–92.
[34] J.Z. Lu, K.Y. Luo, D.K. Yang, X.N. Cheng, J.L. Hu, F.Z. Dai, H. Qi, L. Zhang, J.S. Zhong, Q.W. Wang, Y.K. Zhang, Corros. Sci. 60 (2012) 145–152.

Materials and Design 63 (2014) 488–492

Contents lists available at ScienceDirect

Materials and Design

journal homepage: www.elsevier.com/locate/matdes

Feasibility study on preparation of coatings on Ti–6Al–4V by combined ultrasonic impact treatment and electrospark deposition

Yang Liu, Dongpo Wang *, Caiyan Deng, Lixing Huo, Lijun Wang, Shu Cao

Tianjin Key Laboratory of Advanced Joining Technology, School of Materials Science and Engineering, Tianjin University, Tianjin 300072, PR China

ARTICLE INFO

Article history:
Received 10 April 2014
Accepted 26 June 2014
Available online 8 July 2014

Keywords:
Coating
Ultrasonic impact treatment
Electrospark processing
Amorphous phase
Residual stress
Wear

ABSTRACT

A novel method combining ultrasonic impact treatment (UIT) with electrospark deposition was developed to prepare coatings on Ti–6Al–4V substrates. The microstructure, phase composition, residual stress, microhardness, and wear performance of the coating were studied, and new amorphous and nanocrystalline phases (titanium carbide nitride and iron titanium oxide) were found. In addition, the residual stress in the coating and in the substrate near the coating is compressive stress. The maximum compressive residual stress is about −717 MPa, and its depth is about 470 μm. Because of contributions from multiple factors, the wear volume loss of the sample subjected to combined UIT and electrospark processing was reduced by four orders of magnitude compared with that of the base material.

1. Introduction

Titanium and its alloys are widely used in aviation and space technology because of their excellent mechanical properties (high strength and fatigue resistance) and chemical stability (corrosion resistance). However, titanium alloys have poor tribological properties, which reduce their scope of possible usage [1]. To enhance the wear resistance of the material, many surface modification methods have been developed, such as mechanical milling [2], powder sintering [3], electrospark deposition [4], physical vapor deposition [5], plasma immersion ion implantation [6], laser cladding [7], and micro-arc discharge oxidation [8].

Ultrasonic impact treatment (UIT) [9] was originally developed as a method to relax residual welding stress, reduce the stress concentration coefficient of the weld toe, and form compressive residual stress to improve the fatigue performance of the welded structure [10–13]. In recent years, UIT and its variants have been used for surface self-nanocrystallization modification of materials [14]. However, because UIT is a surface mechanical treatment that does not alter the elemental composition, the application range of UIT surface modification is significantly limited. Compared to UIT, electrospark deposition can easily transfer electrodes or other elements to the target [15,16]. However, it creates a molten pool during conventional deposition, and the tensile residual stress in the coating due to the solidification of the molten pool can have large potential negative effects on the wear, fatigue, and stress corrosion performance [17].

This short communication explores the feasibility of the preparation of coatings by combined UIT and electrospark deposition. The microstructure, microhardness, residual stress, and wear performance of the coating are investigated in detail.

2. Experiment and principle

A self-developed machine for combined UIT and electrospark deposition was used to prepare the coatings. A typical photograph of the combined UIT and electrospark processing is shown in Fig. 1a. The principle of the combined processing equipment can be described as follows (Fig. 1b). The ultrasonic transducer converts electrical energy from the ultrasonic generator into ultrasonic vibration with a frequency of 20 kHz. Under a static pressure, the shock ball vibrates rapidly between the ultrasonic transducer and the target surface. The shock ball was made of steel (GCr15) and had a diameter of 15 mm. Its chemical composition (in wt.%) is 0.98% C, 1.51% Cr, 0.15% Si, 0.36% Mn and balance Fe. To combine the electrospark process with UIT, the target and shock ball were connected to the anode and cathode, respectively, of a DC power during the UIT.

The principle of the combined process is shown in Fig. 1c. When the shock ball touches the target (impact process), there is a short in the circuit. During the impact process, various changes occur in target surface, such as plastic deformation and the introduction of compressive residual stress. Then, when the shock ball bounces off

* Corresponding author. Fax: +86 22 27405889.
E-mail address: wangdp@tju.edu.cn (D. Wang).

http://dx.doi.org/10.1016/j.matdes.2014.06.061
0261-3069/

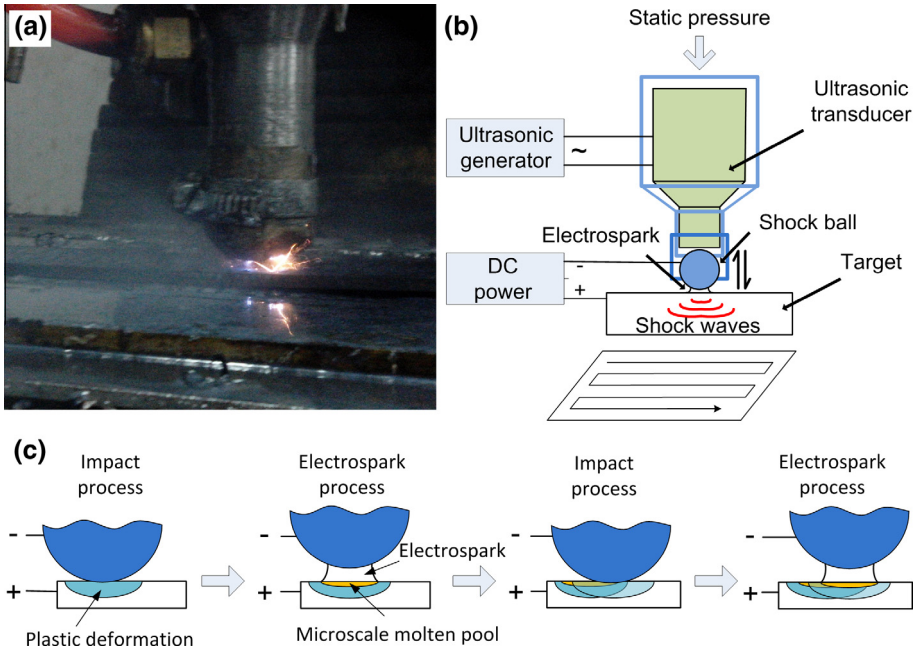

Fig. 1. (a) Typical photograph of the combined process, and (b) schematic diagram of the experiment, and (c) principle of the combined UIT and electrospark process.

the target, electrosparks form between them (electrospark process). This process is equivalent to the contact arc ignition process in arc welding. A microscale molten pool is formed on the surface of target because of the electrospark heating, while the cooling liquid and air in the electrospark area are ionized. Thus, there are many elements from the substrate, electrode, cooling liquid, and air in the microscale molten pool. During the subsequent impact process, the electrospark is extinguished. The surrounding cooling liquid causes rapid solidification of the microscale molten pool. Meanwhile, the target is again subjected to UIT. Then, the shock ball bounces off the target, and the electrospark appears again. The impact process and electrospark process continue in cycles, which constitute the combined process.

A Ti–6Al–4V substrate with the thickness of 3 mm was cut into a rectangle with dimensions of 60 mm × 30 mm and ground using SiC abrasive paper to a 600 grit finish for combined UIT and electrospark processing. Its chemical composition (in wt.%) is 90.31% Ti, 6.13% Al and 3.56% V. The details of the parameters in the combined process are listed in Table 1. The cooling liquid was the cutting fluid for electrical discharge machining.

The cross-sectional microstructure of the coating was observed by scanning electron microscopy (SEM) after metallographic polishing and etching with Kroll's reagent (2 vol% HF and 10 vol% HNO_3 in H_2O). The high-resolution images of the microstructure were obtained by transmission electron microscopy (TEM). The samples for TEM were scraped from the coatings. The phase compositions in the coatings were studied by X-ray diffraction (XRD). The residual stresses at the surface and subsurface of the coatings were determined by applying standard XRD techniques using shifts of XRD peaks with the $\sin^2\psi$ method. Lattice strain measurements were carried out using Cu/Kα radiation at the {1 1 4}-planes of the hexagonal α-phase. The depth profiles of subsurface residual stress were determined by successive electrolytic material removal. For the stress calculation, the Poisson's ratio and elastic modulus of the specimen were set to be 0.31 and 119 GPa, respectively. After polishing, the microhardness distribution of the coatings was measured by a digital microhardness tester (MHV-2000) under an applied load of 0.49 N for a load time of 15 s. The wear tests were carried out on a ring-on-block tester using 43.4 mm diameter GCr15 rings as counterparts. Unlubricated wear tests with a sliding distance of 436 m were carried out with a sliding speed of 0.45 m/s and normal loads of 50 N at room temperature. The widths of the wear scars, which were used to calculate the wear volume loss, were measured by optical microscope. Each test was carried out three times.

3. Results and discussion

Fig. 2 shows the typical cross-sectional microstructure and the titanium and iron distributions in the coatings. After it was treated by combined UIT and electrospark processing, the sample consisted of an outer coating, an inner plastic deformation region, and the substrate (see Fig. 2a). It is noted that the coating has a thickness of about 12 μm, is very compact without obvious cracks, and is bonded to the substrate tightly. The coating was formed by rapid solidification of the microscale molten pool, and the plastic deformation layer was formed by the impact process. Compared with the grains in the heat-affected zone between the coating and substrate formed during laser cladding [7], the grains in the region between the coating and substrate in the sample treated by combined UIT and electrospark processing did not grow. In contrast, they were obviously refined as a result of the severe plastic deformation during the impact process, which may improve the toughness of the bonding zone between the coating and substrate. The coating mainly consists of titanium and iron, as shown in

Table 1
Details of the parameters in the combined UIT and electrospark process.

Transducer amplitude (μm)	Static pressure (N)	Feeding velocity of UIT (mm/min)	Step distance of UIT (mm)	Current of electrospark (A)
20	100	185	0.3	15

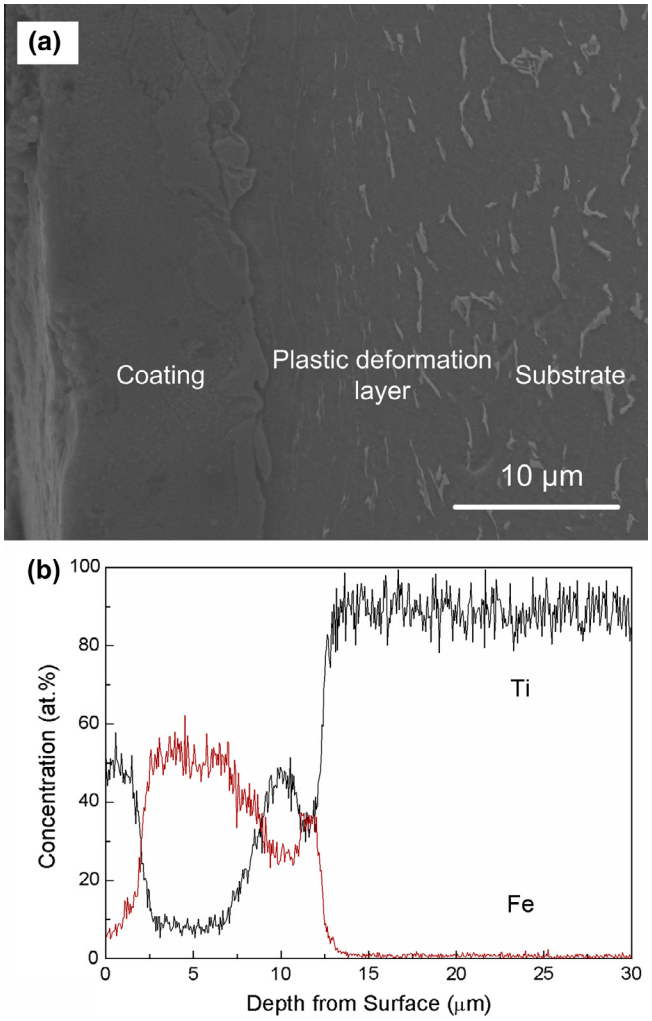

Fig. 2. (a) Cross-sectional microstructure and (b) titanium/iron distributions along the depth direction in the coating.

Fig. 2b, because the cathode of the electrospark equipment is the shock ball, which contains lots of iron. This result demonstrates that the iron is transferred from the cathode to the microscale molten pool on the target surface and is mixed with titanium during the electrospark process. It can be seen that there is a transition layer with a thickness of about several microns, which confirms the metallurgical bonding between the coating and substrate. As is the case in micro-arc discharge oxide coating [8], some elements of the coating come from the substrate, which can improve the bonding strength between the coating and substrate significantly. On the other hand, the coating obtained with the combined process is more heterogeneous than those produced by powder sintering [3] because of the rapid solidification of the coating when the electrospark is extinguished. Although the wear resistance of the heterogeneous coating is nonuniform, this combined process is also worthy of attention because it requires only simple equipment and provides good metallurgic bonding.

Fig. 3 shows TEM images of the coating, in which both amorphous phases and nanocrystals can be observed. The formation process for the amorphous phases can be described as follows. During the electrospark process, the microscale molten pool appears on the target surface as a result of melting of the substrate surface metal and cathode material. During the subsequent impact process, the electrospark is extinguished, so the microscale molten pool, which is surrounded by cooling liquid, rapidly solidifies

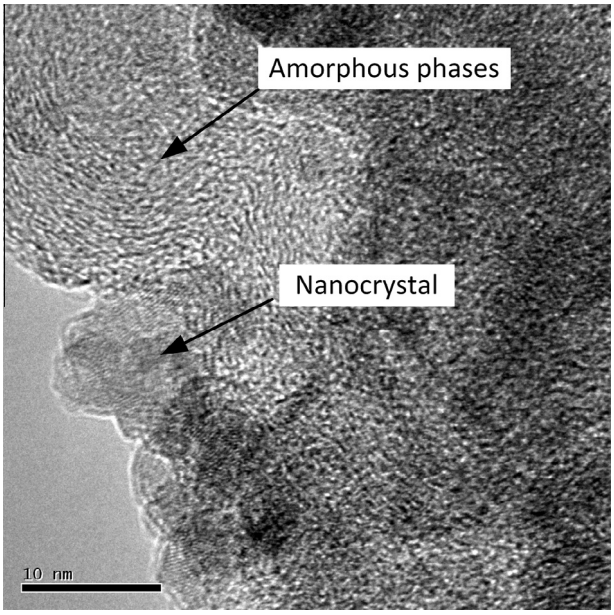

Fig. 3. TEM image of the coating.

under a large temperature gradient. This large temperature gradient allows amorphous phases to form. Meanwhile, the shock waves can provide convenient environments for the formation of nanocrystals. The amorphous phases and nanocrystals in the coating greatly improve the hardness and wear resistance of the material. The detailed results are discussed later. The results of the elemental analysis of the coating are listed in Table 2. It can be seen the coating layer has a lower titanium content than the substrate, and new elements such as iron, carbon, nitrogen, and oxygen appear. The iron comes from the cathode, the carbon comes from the cooling liquid, and the nitrogen and oxygen come from the ionized air.

Fig. 4 shows the XRD patterns for the coating and base material (BM). For the coating, the intensity of Ti phase is lower than that of the new phases ($C_{0.3}N_{0.7}Ti$ and Fe_2Ti_4O). This indicates that the main surface phases of the coating are titanium carbide nitride and iron titanium oxide. Besides the appearance of new phases, all diffraction peaks from the coating are broadened. This suggests that there is grain refinement or/and microstrain due to the rapid solidification and severe plastic deformation of the coating during the impact process. This mechanism is in good agreement with the TEM observations of amorphous phases and nanocrystals in the coating and with the SEM observation of a plastic deformation layer under the coating. This process is different from that occurring in the conventional coating method [6,15].

The residual stress in coatings has been studied extensively [17]. During powder sintering, the surface layer and the substrate showed different shrinkages, as measured by the changes in their sizes [3]. Moreover, Ahmaniemi et al. found that residual stress states were correlated with other coating properties such as the microhardness, porosity, microstructure, and dry abrasion wear resistance [18]. Compared to the conventional coating process, the combined UIT and electrospark process has the significant advantage of producing a large compressive residual stress field

Table 2
Results of the elemental analysis of the coating.

Element	C	N	O	Al	Ti	V	Fe
Atomic %	6.639	26.347	10.599	6.872	34.417	3.197	11.929

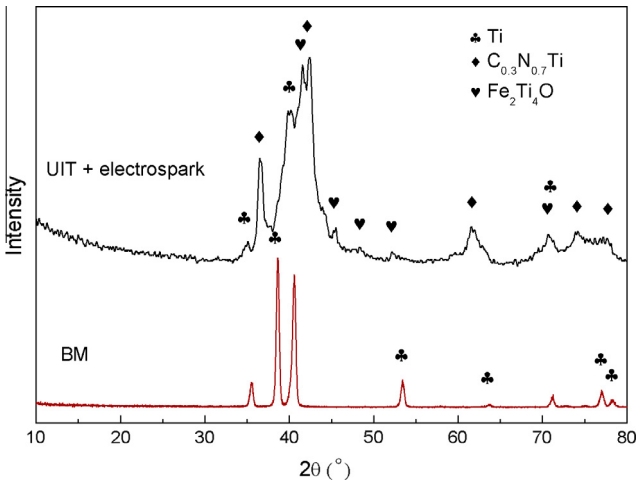

Fig. 4. XRD patterns for the sample treated by the combined UIT and electrospark processing and for the base material.

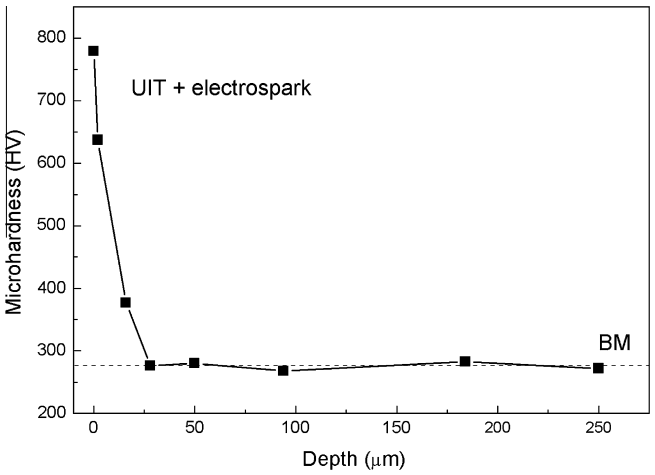

Fig. 6. Microhardness profiles of the sample treated by combined UIT and electrospark processing and of the base material.

in the coating and substrate. Previous studies have concluded that compressive residual stress is beneficial for improving the wear [18], fatigue [19], and stress corrosion [20] resistance of components. Fig. 5 shows the changes in residual stress along the depth direction before and after the combined UIT and electrospark processing. It is clearly observed that there is almost no residual stress in the base material. In the sample treated using the combined process, the maximum compressive residual stress (−717 MPa) is found on the top surface of the coating, and the effective depth of the compressive residual stress is about 470 μm.

The cross-sectional microhardness profile of the sample subjected to the combined UIT and electrospark processing is given in Fig. 6. The maximum microhardness is about 800 HV on the top surface of the coating. This is due to the amorphous, nanometer-sized titanium carbide nitride and iron titanium oxide phases in the coating. The microhardness is also higher under the coating than in the base material because of the plastic deformation present to a depth of 30 μm.

Fig. 7 shows the wear test results for the sample treated by combined UIT and electrospark processing and for the base material. The wear loss volume was calculated according to Eq. (1):

$$V_k = \frac{D^2}{8} t \left[2\sin^{-1}\frac{b}{D} - \sin\left(2\sin^{-1}\frac{b}{D}\right)\right], \quad (1)$$

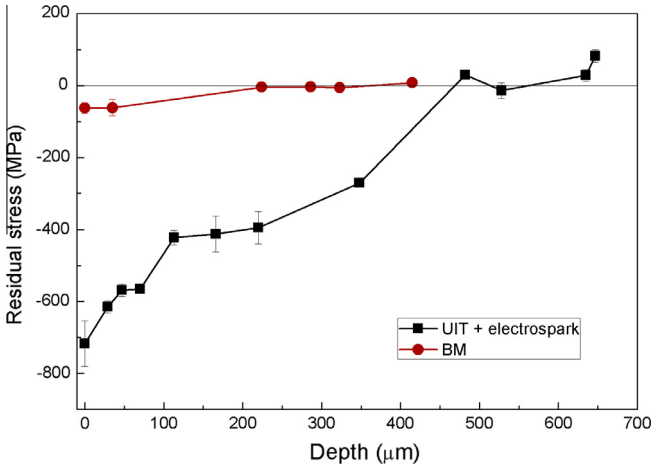

Fig. 5. Residual stress profiles of the sample treated by combined UIT and electrospark processing and of the base material.

where V_k is the wear volume loss (mm^3), D is the diameter of the ring counterparts (mm), t is the width of the wear test sample (mm), and b is the average width of the wear track (mm). The average of the three values measured at the middle and at both ends of the wear track was used in this calculation.

As shown in Fig. 7a, the wear resistance of sample treated by combined UIT and electrospark processing was obviously improved from that of the Ti–6Al–4V base. Although the friction coefficient was quite high, the wear volume loss was reduced by four orders of magnitude. In Fig. 7c, it can be seen that there is an obvious furrow on the wear track, which is a typical characteristic of abrasive wear [3]. Since the hardness of the base material is less than that of the ring counterparts (about 819 HV), the micro-embossment on the surface of the base material was squeezed, and plastic deformation occurred during the wear process. Then, the work-hardened micro-embossment fell away from the base material and became abrasive particles. Therefore, the base material was subjected to cutting by the abrasive particles and micro-embossment on the counterparts, which formed the furrow on the wear track [7].

On the other hand, for the sample subjected to combined UIT and electrospark processing, the wear mechanism is mainly adhesive wear. The hardness of the coating is similar to that of the counterparts, so the coating is not work-hardened or cut by the counterparts. In addition, the existence of iron in the coating led to a strong adhesive effect, so the friction coefficient of the sample treated by combined UIT and electrospark processing is higher than that of the base material. The reason why no cracking appeared on the wear track, which is a typical characteristic of fatigue wear, could be that the amorphous phases and nanocrystals, along with the compressive residual stress, enhanced the toughness of the material. From Fig. 7d, we can see visible adhesive marks (A) and fragments from the counterparts (B) formed by adhesive wear. Thus, this experiment demonstrates that the coating exhibits excellent wear resistance.

The improvement in the wear resistance is attributed to a combination of many factors. Although the hardness of the coating is increased by the addition of titanium carbide nitride and iron titanium oxide, these phases also reduce the toughness of the coating sharply, which may result in cracking and spalling of the coating. The existence of amorphous phases and nanocrystals enhances the strength, hardness, and toughness of the coatings. Therefore, these phases combined with the compressive residual stress field not only provide the coating a high hardness and good wear resistance, but also prevent cracking or spalling.

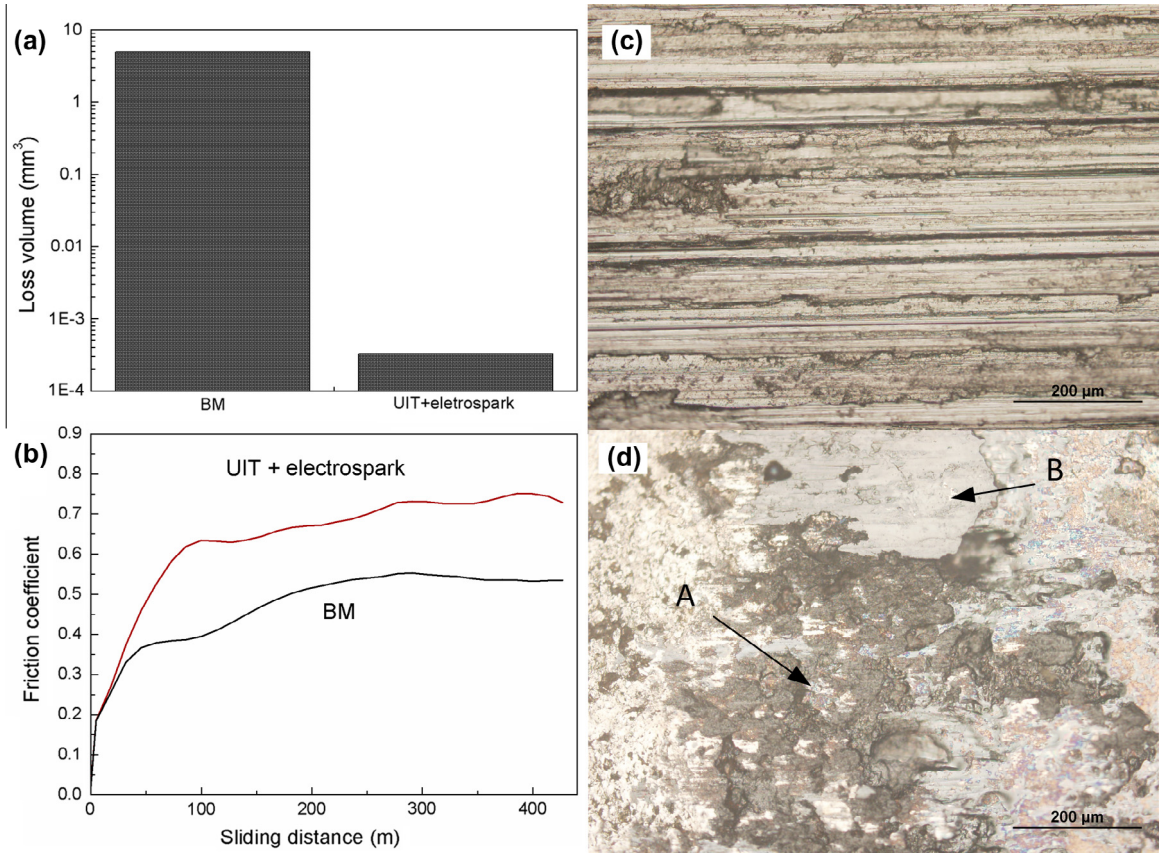

Fig. 7. (a) Wear results, (b) friction coefficient, and wear scars (c) on the base material and (d) on the sample treated by combined UIT and electrospark processing.

4. Conclusions

A combined UIT and electrospark process has been developed to prepare hard and wear-resistant coatings on Ti–6Al–4V substrates. The obtained coating had a thickness of 12 μm. In addition, there are new titanium carbide nitride and iron titanium oxide phases in the coating, which also contains both amorphous phases and nanocrystals. In addition, a compressive residual stress field is formed in and under the coating. These factors all contribute to a significant improvement in the coating wear resistance.

Acknowledgement

The authors are grateful for the support by the National Natural Science Foundation of China (Grant Nos. 51275343 and 51375331).

References

[1] Budzynski P, Youssef AA, Sielanko J. Surface modification of Ti–6Al–4V alloy by nitrogen ion implantation. Wear 2006;261:1271–6.
[2] Romankov S, Komarov SV, Vdovichenko E, Hayasaka Y, Hayashi N, Kaloshkin SD, et al. Fabrication of TiN coatings using mechanical milling techniques. Int J Refract Met H 2009;27:492–7.
[3] Hu R-H, Lim J-K. Hardness and wear resistance improvement of surface composite layer on Ti–6Al–4V substrate fabricated by powder sintering. Mater Des 2010;31:2670–5.
[4] Dancer CEJ, Yahya NA, Berndt T, Todd RI, de Portu G. Effect of residual compressive surface stress on severe wear of alumina–silicon carbide two-layered composites. Tribol Int 2014;74:87–92.
[5] Cassar G, Banfield S, Wilson JCA-B, Housden J, Matthews A, Leyland A. Tribological properties of duplex plasma oxidised, nitrided and PVD coated Ti–6Al–4V. Surf Coat Technol 2011;206:395–404.
[6] Abd El-Rahman AM, Raaif M, Mohamed SH, Kolitsch A. Mechanical and ellipsometry measurements of thin TiN layer prepared by PIII. Mater Chem Phys 2012;132:91–5.
[7] Yang Y, Zhang D, Yan W, Zheng Y. Microstructure and wear properties of TiCN/Ti coatings on titanium alloy by laser cladding. Opt Laser Eng 2010;48:119–24.
[8] Nie X, Leyland A, Song HW, Yerokhin AL, Dowey SJ, Matthews A. Thickness effects on the mechanical properties of micro-arc discharge oxide coatings on aluminium alloys. Surf Coat Technol 1999;116:1055–60.
[9] Statnikov ES, Korolkov OV, Vityazev VN. Physics and mechanism of ultrasonic impact. Ultrasonics 2006;44. pp. E533-E8.
[10] Zhao X, Wang D, Huo L. Analysis of the S–N curves of welded joints enhanced by ultrasonic peening treatment. Mater Des 2011;32:88–96.
[11] Abdullah A, Malaki M, Eskandari A. Strength enhancement of the welded structures by ultrasonic peening. Mater Des 2012;38:7–18.
[12] Wang T, Wang D, Huo L, Zhang Y. Discussion on fatigue design of welded joints enhanced by ultrasonic peening treatment (UPT). Int J Fatigue 2009;31:644–50.
[13] Yin D, Wang D, Jing H, Huo L. The effects of ultrasonic peening treatment on the ultra-long life fatigue behavior of welded joints. Mater Des 2010;31:3299–307.
[14] Ting W, Dongpo W, Gang L, Baoming G, Ningxia S. Investigations on the nanocrystallization of 40Cr using ultrasonic surface rolling processing. Appl Surf Sci 2008;255:1824–9.
[15] Xie Y-j, Wang M-c. Isothermal oxidation behavior of electrospark deposited MCrAlX-type coatings on a Ni-based superalloy. J Alloy Compd 2009;480:454–61.
[16] Zamulaeva EI, Levashov EA, Kudryashov AE, Vakaev PV, Petrzhik MI. Electrospark coatings deposited onto an Armco iron substrate with nano- and microstructured WC-Co electrodes: deposition process, structure, and properties. Surf Coat Technol 2008;202:3715–22.
[17] Montay G, Cherouat A, Nussair A, Lu J. Residual stresses in coating technology. J Mater Sci Technol 2004;20:81–4.
[18] Ahmaniemi S, Vippola M, Vuoristo P, Mäntylä T, Buchmann M, Gadow R. Residual stresses in aluminium phosphate sealed plasma sprayed oxide coatings and their effect on abrasive wear. Wear 2002;252:614–23.
[19] Ren XD, Zhan QB, Yang HM, Dai FZ, Cui CY, Sun GF, et al. The effects of residual stress on fatigue behavior and crack propagation from laser shock processing-worked hole. Mater Des 2013;44:149–54.
[20] Ahmadi-Pidani R, Shoja-Razavi R, Mozafarinia R, Jamali H. Improving the hot corrosion resistance of plasma sprayed ceria–yttria stabilized zirconia thermal barrier coatings by laser surface treatment. Mater Des 2014;57:336–41.